AIP | The Journal of Chemical Physics

Modeling molecule-plasmon interactions using quantized radiation fields within time-dependent electronic structure theory

Daniel R. Nascimento and A. Eugene DePrince III

Citation: The Journal of Chemical Physics **143**, 214104 (2015); doi: 10.1063/1.4936348
View online: http://dx.doi.org/10.1063/1.4936348
View Table of Contents: http://scitation.aip.org/content/aip/journal/jcp/143/21?ver=pdfcov
Published by the AIP Publishing

Modeling molecule-plasmon interactions using quantized radiation fields within time-dependent electronic structure theory

Daniel R. Nascimento and A. Eugene DePrince III[a)]
Department of Chemistry and Biochemistry, Florida State University, Tallahassee, Florida 32306-4390, USA

(Received 12 September 2015; accepted 11 November 2015; published online 1 December 2015)

We present a combined cavity quantum electrodynamics/*ab initio* electronic structure approach for simulating plasmon-molecule interactions in the time domain. The simple Jaynes-Cummings-type model Hamiltonian typically utilized in such simulations is replaced with one in which the molecular component of the coupled system is treated in a fully *ab initio* way, resulting in a computationally efficient description of general plasmon-molecule interactions. Mutual polarization effects are easily incorporated within a standard ground-state Hartree-Fock computation, and time-dependent simulations carry the same formal computational scaling as real-time time-dependent Hartree-Fock theory. As a proof of principle, we apply this generalized method to the emergence of a Fano-like resonance in coupled molecule-plasmon systems; this feature is quite sensitive to the nanoparticle-molecule separation and the orientation of the molecule relative to the polarization of the external electric field. © *2015 AIP Publishing LLC.* [http://dx.doi.org/10.1063/1.4936348]

I. INTRODUCTION

Interactions between localized surface plasmons and nearby molecules have long been a subject of intense scientific inquiry. The enhanced electric fields associated with a plasmon excitation can have a dramatic effect on the optical properties of nearby molecules, leading to a variety of familiar processes, including surface-enhanced Raman scattering[1–6] and other enhanced absorption/emission events.[7–16] Further, the presence of the dipole emitter can have a profound effect on the character of the plasmon excitation. Examples of complex feedback and optical interference in coupled systems include Fano resonances,[17–20] dipole-induced transparencies,[21] and the excitation of a plasmon mode via electron-hole pair annihilation.[22–24] The broad applicability of these phenomena has spurred decades of research aimed at understanding and controlling the interactions between plasmonic nanomaterials and individual quantum emitters.

Practical theoretical models for plasmon-molecule interactions must address a number of technical challenges, the first of which is the large disparity in length scales in such systems. A variety of multiscale approaches have been proposed wherein the plasmonic material is treated classically, and the molecular component is treated quantum mechanically. Metallic nanostructures are often described by the discrete dipole approximation[25] or finite-difference time-domain methods,[26] while the molecular component can be treated using Hartree-Fock/density functional theory (DFT)[27–30] or many-body Green's function methods.[31–35] Alternatively, polarizable continuum models can describe the surface charges of a plasmonic particle coupled to a molecule that, again, should be treated quantum mechanically.[36–42]

A second challenge stems from the fact that the very intense electric fields associated with the plasmon resonance may necessitate a quantum-mechanical treatment of the molecule that moves beyond linear-response theory. With a few exceptions, molecular system components are almost universally treated within the frequency domain and in the linear-response regime. Such strategies may be insufficient to describe molecules subjected to intense fields, such as those that would be present between two closely spaced nanoparticles (NPs). Some studies have explored the utility of real-time time-dependent quantum mechanical approaches, which could indeed capture the nonlinear optical properties of molecules near plasmonic nanomaterials,[27,30] but a general, real-time, and fully quantum-mechanical description of the interplay of competing optical pathways in the molecule and the plasmonic material is still lacking. A quantum-mechanical treatment of the plasmon excitation is sometimes necessary to describe the nonlinear optical properties of coupled plasmon-molecule systems.[18,43,44]

Recently, several groups have modeled interactions between plasmonic materials and dipole emitters within the framework of cavity quantum electrodynamics (CQED);[17–20] a plasmonic nanoparticle can serve as the cavity, and the fields associated with the plasmon resonance are quantized. CQED provides a simple yet powerful methodology for describing a variety of nonlinear effects in hybrid nanostructures, including the emergence of Förster resonance energy transfer[18] and the "reversal" of a Fano resonance by manipulating the energy content of an oscillating external electric field.[17] Further, the quantum-mechanical description of the plasmon excitation afforded by CQED is absolutely necessary to capture some phenomena, such as entangled plasmon excitations in metal nanoparticle heterodimers.[45]

Existing CQED-inspired studies of hybrid nanostructures typically describe the system with a Jaynes-Cummings-type model Hamiltonian.[46] In general, the plasmon excitation is represented as a single dipolar cavity mode characterized by a dipole oscillator strength, an excitation frequency, and

a)Electronic address: deprince@chem.fsu.edu

a damping rate. The relevant operators are then expanded in an orthonormal basis of photon-number states. Dipole emitters are typically approximated as two-level systems, again characterized by an excitation energy, a damping rate, and a dipole oscillator strength. A CQED-based approach to plasmon-molecule interactions has the potential to be of far more general utility, so, in this paper, we introduce a fully *ab initio* electronic Hamiltonian into the CQED formalism. This treatment should provide a more realistic and predictive description of the quantum emitter, as compared to the conventional two-level treatment. As a proof of principle, we apply this generalized method to the resonant coupling between plasmonic nanoparticles and nearby molecules. We explore the emergence of a Fano-like resonance in the coupled system that displays great sensitivity to the orientation of the molecule relative to the nanoparticle and the polarization of the external electric field.

II. THEORY

A. The ground state

We first consider the static (time-independent) interaction of the cavity (the plasmonic particle) and a general molecular system. The plasmon excitation is treated as a three-dimensional quantum harmonic oscillator, characterized by a plasmon resonance energy, a dipole oscillator strength, and a damping rate. The Hamiltonian for the isolated plasmonic particle, $\hat{H}_{\mathrm{p},0}$, is

$$\hat{H}_{\mathrm{p},0} = \sum_{\xi} \omega_{\mathrm{p}}^{\xi} \hat{b}_{\xi}^{\dagger} \hat{b}_{\xi}, \tag{1}$$

where $\omega_{\mathrm{p}}^{\xi}$ represents the frequency of a dipolar plasmon mode in the ξ direction ($\xi \in \{x, y, z\}$), and $\hat{b}_{\xi}^{\dagger}$ ($\hat{b}_{\xi}$) represents a bosonic raising (lowering) operator for the plasmon mode in the ξ direction. In this work, we restrict our considerations to dipolar excitations, but ξ could represent any modes, whether they be dipolar or quadrupolar in nature, a plasmon waveguide mode, or modes corresponding to plasmon excitations centered on different nanoparticles. The raising and lowering operators are defined by their action on different photon number states, where

$$\hat{b}_{\xi}^{\dagger} |A_{\xi}\rangle = (A_{\xi} + 1)^{1/2} |A_{\xi} + 1\rangle, \tag{2}$$

and

$$\hat{b}_{\xi} |A_{\xi}\rangle = (A_{\xi})^{1/2} |A_{\xi} - 1\rangle. \tag{3}$$

Here, $|A_{\xi}\rangle$ represents a state with A_{ξ} quanta in mode ξ. In all of our computations, the plasmonic particle is taken to be spherical, that is, $\omega_{\mathrm{p}}^{x} = \omega_{\mathrm{p}}^{y} = \omega_{\mathrm{p}}^{z}$.

The Hamiltonian for the electronic degrees of freedom of the isolated molecular system, $\hat{H}_{\mathrm{e},0}$, is

$$\hat{H}_{\mathrm{e},0} = \sum_{pq} h_{pq} \hat{a}_{p}^{\dagger} \hat{a}_{q} + \frac{1}{2} \sum_{pqrs} (pr|qs) \hat{a}_{p}^{\dagger} \hat{a}_{q}^{\dagger} \hat{a}_{s} \hat{a}_{r}, \tag{4}$$

where h_{pq} represents the sum of the electron kinetic energy and electron-nucleus potential energy integrals, $(pr|qs)$ represents a two-electron repulsion integral in Mulliken notation, and the operator $\hat{a}^{\dagger}$ ($\hat{a}$) represents a fermionic creation (annihilation) operator. The indices p, q, r, and s run over all spin orbitals.

In the present model, plasmonic and molecular components interact through semiclassical dipole-dipole interactions, and the interaction component of the Hamiltonian, $\hat{H}_{\mathrm{i}}$, is

$$\hat{H}_{\mathrm{i}} = \frac{1}{R^3} \left[\hat{\boldsymbol{\mu}}_{\mathrm{p}} \cdot \hat{\boldsymbol{\mu}}_{\mathrm{e}} - 3 \frac{(\hat{\boldsymbol{\mu}}_{\mathrm{p}} \cdot \mathbf{R})(\mathbf{R} \cdot \hat{\boldsymbol{\mu}}_{\mathrm{e}})}{R^2} \right]. \tag{5}$$

Here, the vector $\mathbf{R}$ defines the separation between the dipoles centered at the plasmonic particle and the molecule; for simplicity, we take the location of the molecular dipole moment to be at the center of mass of the molecule. The molecular dipole operator, $\hat{\boldsymbol{\mu}}_{\mathrm{e}}$, is defined as

$$\hat{\boldsymbol{\mu}}_{\mathrm{e}} = \sum_{\xi} \sum_{p,q} \mu_{pq}^{\xi} \hat{\mathbf{e}}_{\xi} \hat{a}_{p}^{\dagger} \hat{a}_{q}, \tag{6}$$

where μ_{pq}^{ξ} is evaluated in a basis of atomic or molecular orbitals $\{\phi_p\}$ as

$$\mu_{pq}^{\xi} = -\int \phi_{p}^{*} \xi \phi_{q} d\mathbf{r}, \tag{7}$$

and $\hat{\mathbf{e}}_{\xi}$ represents the unit vector in the ξ direction. The plasmon dipole operator, $\hat{\boldsymbol{\mu}}_{\mathrm{p}}$, is

$$\hat{\boldsymbol{\mu}}_{\mathrm{p}} = \sum_{\xi} \mu_{\mathrm{p}}^{\xi} \hat{\mathbf{e}}_{\xi}, \tag{8}$$

where

$$\mu_{\mathrm{p}}^{\xi} = d_{\mathrm{p}}^{\xi} (\hat{b}_{\xi}^{\dagger} + \hat{b}_{\xi}). \tag{9}$$

Here, d_{p}^{ξ} represents a transition dipole moment for the plasmon excitation in the ξ direction.

In the absence of an external electric field, the Hamiltonian for the coupled plasmon-molecule system is

$$\hat{H}_0 = \hat{H}_{\mathrm{e},0} + \hat{H}_{\mathrm{p},0} + \hat{H}_{\mathrm{i}}, \tag{10}$$

which carries explicit two-body terms in both $\hat{H}_{\mathrm{e},0}$ and $\hat{H}_{\mathrm{i}}$. The two-body nature of the interaction term can be simplified by assuming that the total wave function for the coupled system is separable into a product of plasmonic and electronic wave functions as

$$|\Psi\rangle = |\Psi_{\mathrm{e}}\rangle |\Psi_{\mathrm{p}}\rangle. \tag{11}$$

Within this approximation, we rewrite the interaction term as a sum of two types of interactions

$$\hat{H}_{\mathrm{i}} = \frac{1}{2} \left(\hat{H}_{\mathrm{i}}^{\mathrm{p}\to\mathrm{e}} + \hat{H}_{\mathrm{i}}^{\mathrm{e}\to\mathrm{p}} \right), \tag{12}$$

where $\hat{H}_{\mathrm{i}}^{\mathrm{p}\to\mathrm{e}}$ represents the potential felt by the electrons in the molecule due to the presence of the plasmon dipole, and $\hat{H}_{\mathrm{i}}^{\mathrm{e}\to\mathrm{p}}$ represents the potential felt by the nanoparticle due to the presence of the molecular dipole. The electron → plasmon potential operator is similar to the semiclassical dipole-dipole potential operator considered above,

$$\hat{H}_{\mathrm{i}}^{\mathrm{e}\to\mathrm{p}} = \frac{1}{R^3} \left[\hat{\boldsymbol{\mu}}_{\mathrm{p}} \cdot \langle \hat{\boldsymbol{\mu}}_{\mathrm{e}} \rangle - 3 \frac{(\hat{\boldsymbol{\mu}}_{\mathrm{p}} \cdot \mathbf{R})(\mathbf{R} \cdot \langle \hat{\boldsymbol{\mu}}_{\mathrm{e}} \rangle)}{R^2} \right], \tag{13}$$

except that the electronic dipole operator has been replaced by an expectation value. The potential felt by the electrons due to the presence of the nanoparticle is

$$\hat{H}_{\mathrm{i}}^{\mathrm{p}\to\mathrm{e}} = -\sum_{p,q}\left[\int \phi_p^*\left(\frac{\mathbf{r}_\mathrm{e}-\mathbf{r}_\mathrm{p}}{|\mathbf{r}_\mathrm{e}-\mathbf{r}_\mathrm{p}|^3}\right)\phi_q d\mathbf{r}_\mathrm{e}\right]\cdot\langle\hat{\boldsymbol{\mu}}_\mathrm{p}\rangle\hat{a}_p^\dagger\hat{a}_q, \tag{14}$$

where $\mathbf{r}_\mathrm{e}$ and $\mathbf{r}_\mathrm{p}$ represent the coordinates of the electron and the plasmonic particle, respectively. We will demonstrate in Sec. IV that the mean-field description of the plasmon-molecule interactions implied by Eq. (11) yields a description of the dynamics that is numerically indistinguishable from the explicit many-body description in the noninteracting limit, and the slight differences that emerge in interacting systems can be attributed to the apparent infeasibility of the two-body plasmon-molecule reduced-density-matrix (RDM) associated with the explicit many-body description.

The electronic wave function, $|\Psi_\mathrm{e}\rangle$, is approximated as a single Slater determinant. Obtaining the ground-state energy and wave function for the coupled system then requires a modified Hartree-Fock self-consistent field (SCF) procedure, which is outlined as follows:

1. Build the matrix-representation of the field-free operators for the plasmon excitation ($\hat{H}_{\mathrm{p},0}$, $\hat{H}_{\mathrm{i}}^{\mathrm{e}\to\mathrm{p}}$, and $\hat{\boldsymbol{\mu}}_\mathrm{p}$) in a basis of photon number states.
2. Construct the field-free plasmon excitation Hamiltonian: $\hat{H}'_\mathrm{p} = \hat{H}_{\mathrm{p},0} + \hat{H}_{\mathrm{i}}^{\mathrm{e}\to\mathrm{p}}$ in the current basis.
3. Build the Fock matrix and include the potential due to the presence of the nanoparticle dipole: $\hat{H}_{\mathrm{i}}^{\mathrm{p}\to\mathrm{e}}$.
4. Diagonalize the Fock matrix to determine new molecular orbitals.
5. Transform each operator for the plasmonic component to the basis that diagonalizes $\hat{H}'_\mathrm{p}$.
6. Repeat steps 2–5 until convergence.

Mutual polarization effects are included self-consistently upon convergence of this modified SCF procedure. Note that the transformation performed in Step 5 does not change the plasmon excitation energies.

B. Time dependence

We next consider the dynamical behavior of the coupled system in the presence of an oscillating external electric field. Specifically, we seek equations of motion (EOMs) for the one-body RDMs for the electronic and plasmonic components of the system, defined as

$$\rho_q^p = \langle\Psi|\hat{a}_p^\dagger\hat{a}_q|\Psi\rangle, \tag{15}$$

and

$$\rho(\xi)_B^A = \langle\Psi|\hat{b}(\xi)_A^\dagger\hat{b}(\xi)_B|\Psi\rangle, \tag{16}$$

respectively. Here, we differentiate between electronic basis functions and photon number states with lower- and upper-case indices, respectively. We have also introduced a new set of bosonic operators defined in terms of raising and lowering operators acting on the photon vacuum state, $|0\rangle$,

$$\hat{b}(\xi)_A^\dagger = \frac{1}{\sqrt{A!}}\left(\hat{b}_\xi^\dagger\right)^A|0\rangle, \tag{17}$$

and

$$\hat{b}(\xi)_A = \left(\hat{b}(\xi)_A^\dagger\right)^\dagger. \tag{18}$$

Time-dependent Hamiltonian operators that govern the dynamics of the electronic and plasmonic system components, $\hat{H}_\mathrm{e}(t)$ and $\hat{H}_\mathrm{p}(t)$, can be defined as

$$\hat{H}_\mathrm{e}(t) = \hat{H}_{\mathrm{e},0} + \hat{H}_{\mathrm{i}}^{\mathrm{p}\to\mathrm{e}} - \hat{\boldsymbol{\mu}}_\mathrm{e}\cdot\mathcal{E}(t), \tag{19}$$

and

$$\hat{H}_\mathrm{p}(t) = \hat{H}_{\mathrm{p},0} + \hat{H}_{\mathrm{i}}^{\mathrm{e}\to\mathrm{p}} - \hat{\boldsymbol{\mu}}_\mathrm{p}\cdot\mathcal{E}(t), \tag{20}$$

where $\mathcal{E}(t)$ represents a time-dependent external electric field. The time derivative of the expectation values of the one-body reduced-density operators $\hat{a}_p^\dagger\hat{a}_q$ and $\hat{b}(\xi)_A^\dagger\hat{b}(\xi)_B$ is given by the commutators of these operators with the appropriate Hamiltonian; the equations of motion for the electronic and plasmonic one-body RDMs are

$$i\frac{d}{dt}\rho_q^p = \langle\Psi|[\hat{a}_p^\dagger\hat{a}_q, \hat{H}_\mathrm{e}(t)]|\Psi\rangle, \tag{21}$$

and

$$i\frac{d}{dt}\rho_B^A(\xi) = \langle\Psi|[\hat{b}(\xi)_A^\dagger\hat{b}(\xi)_B, \hat{H}_\mathrm{p}(t)]|\Psi\rangle, \tag{22}$$

respectively. The right-hand side of Eq. (21) is a function of both the one-electron RDM and the two-electron RDM, but under the assumption that the electronic wave function is representable by a single Slater determinant, the correlated part of the two-electron RDM vanishes, and Eq. (21) reduces to the EOM for the one-electron RDM according to time-dependent Hartree-Fock (TDHF) theory (to within a minus sign), augmented by the presence of the oscillating dipole moments associated with the plasmon excitations. Equation (22) represents three EOMs for dipolar plasmon excitations polarized in three spatial directions. The computational cost of propagating Eq. (21) is dominated by the repeated construction of the Fock matrix, which scales computationally as the fourth-power with the size of the one-electron basis set. Equation (22) scales computationally with the square of the number of photon number states included in the computation; in this work, this number is limited to 50, and the computational cost of the entire procedure is dominated by the fourth-power scaling of Eq. (21). Hence, the formal scaling of the present method is equivalent to that of a standard real-time TDHF procedure. Note also that the basis of 50 photon number states is far larger than is necessary, given the strength of the external electric field used in these studies; the simulations presented in Sec. IV are fully converged with the inclusion of only 10 photon number states.

Finally, the decay of the plasmon excitation is captured by a Liouvillian superoperator, written in Lindblad form[47] as

$$\begin{aligned}\hat{L}(\hat{b}(\xi)_A^\dagger\hat{b}(\xi)_B) = -\frac{\gamma_\mathrm{p}^\xi}{2}\Big(&\hat{b}_\xi^\dagger\hat{b}_\xi\hat{b}(\xi)_A^\dagger\hat{b}(\xi)_B \\ &+ \hat{b}(\xi)_A^\dagger\hat{b}(\xi)_B\hat{b}_\xi^\dagger\hat{b}_\xi - 2\hat{b}_\xi\hat{b}(\xi)_A^\dagger\hat{b}(\xi)_B\hat{b}_\xi^\dagger\Big),\end{aligned} \tag{23}$$

where γ_p^ξ represents a damping rate for the plasmonic excitation in the ξ direction. Note that the plasmon damping rate is typically much larger than the molecular spontaneous

emission and dephasing rates, so we ignore dissipation in Eq. (21). The EOM for the plasmon 1-RDM takes the final form

$$i\frac{d}{dt}\rho_B^A(\xi) = \langle\Psi|[\hat{b}(\xi)_A^\dagger \hat{b}(\xi)_B, \hat{H}_\mathrm{p}(t)]|\Psi\rangle + i\langle\Psi|\hat{L}(\hat{b}(\xi)_A^\dagger \hat{b}(\xi)_B)|\Psi\rangle. \quad (24)$$

III. COMPUTATIONAL DETAILS

The ground-state wave function was obtained from a modified version of the restricted Hartree-Fock algorithm in the `Psi4` electronic structure package,[48] and the algorithm for the time evolution of the system was implemented as a plugin to `Psi4`. For all computations, the one-electron basis set was the 6-31G basis set. All computations were performed using a z-polarized laser pulse centered at the plasmon resonance frequency with a Gaussian envelope, a full width at half maximum of 10 fs, and an intensity of 5×10^6 V/m. The EOMs were integrated using the fourth-order Runge-Kutta numerical integrator implemented in the Boost library using time step of 0.05 a.u. (≈0.0012 fs).

Parameters for the plasmon excitation (ω_p^ξ, d_p^ξ, and γ_p^ξ) were initially obtained by fitting the simulated extinction cross sections for isolated 20 nm gold and silver nanoparticles to those obtained from Mie theory, assuming the bulk metal optical constants of Johnson and Christy.[49] For coupled molecule-plasmon systems, the plasmon excitation frequencies were then slightly modified to be in resonance with certain molecular electronic excitations; further details are provided below.

IV. RESULTS AND DISCUSSION

We first consider the interaction of a 20 nm gold NP and a simple molecule: Li_2 with bond length of 2 Å. The dipolar plasmon resonance was shifted slightly to be in resonance with the $\Sigma_u^+ \leftarrow \Sigma_g^+$ excitation of Li_2 at 2.47 eV, as predicted at the TDHF/6-31G level of theory. Here, the interplay between the broad plasmonic and narrow molecular excitations may lead to a Fano-like transparency dip in the scattering cross section for the coupled system.[17] Hence, this case will serve as a validation of the present CQED-inspired approach to plasmon-molecule interactions. Figure 1 illustrates the scattering cross section for each component of the coupled system, as well as the geometry of the system and the polarization of the external electric field. The molecule-nanoparticle separation, D, is defined as the distance from the center of mass of the molecule to the "surface" of the nanoparticle. Note that, in the present model, the plasmon excitation takes the form of a polarizable point dipole, and the "surface" merely reflects the underlying parametrization of the plasmon excitation Hamiltonian; these parameters were initially determined from a Mie theory description of a gold particle with a radius of 10 nm. The scattering cross sections for each component of the system are defined by[50]

$$\sigma_\mathrm{sca}(\omega) = \frac{k^4}{6\pi\epsilon_0^2}|\alpha(\omega)|^2, \quad (25)$$

where the wavevector, $k = \epsilon_\mathrm{med}^{1/2}\omega/c$, and the relative dielectric constant of the surrounding medium, ϵ_med, is taken to be unity, throughout. The polarizability, $\alpha(\omega)$, is given by

$$\alpha(\omega) = \frac{\int_0^T e^{i\omega t}\mu(t)dt}{\int_0^T e^{i\omega t}\mathcal{E}(t)dt}, \quad (26)$$

where $\mu(t)$ represents the time-dependent dipole signal for either the molecule or the nanoparticle, and T represents the total simulation time.

As expected, the nanoparticle scattering cross sections presented in Fig. 1 display a transparency dip, the character of which depends on the molecule-nanoparticle distance and the alignment of the external electric field and the molecular axis. This feature emerges despite the nearly negligible magnitude of the molecular scattering cross section relative to that of the isolated nanoparticle; this striking sensitivity has recently been explored as a tool for single-molecule detection[51,52] and molecular rulers.[53] Figures 1(a)-1(d) illustrate the dependence of the line shape on the molecule-nanoparticle separation. The transparency dip is most pronounced at small D and vanishes at infinite separation. Figures 1(e)-1(h) demonstrate the sensitivity of the line shape to the relative orientation of the molecule and the polarization of the external electric field (the angle, θ). Because the $\Sigma_u^+ \leftarrow \Sigma_g^+$ transition dipole moment is aligned with the molecular axis, the coupling between the molecule and nanoparticle is maximized when the molecular axis is parallel to the external electric field [Fig. 1(e)]. Similarly, the resonance at 2.47 eV vanishes when the molecule and field are aligned perpendicularly [Fig. 1(h)]. An additional feature emerges at 2.67 eV for $\theta = 60°$–$90°$, when the Π_u state of Li_2 can be accessed; the alignment of the transition dipole moment for the $\Pi_u \leftarrow \Sigma_g^+$ transition is perpendicular to the molecular axis. The presence of this feature highlights the benefits of the present *ab initio* description of the molecular component; it emerges naturally without any prior knowledge of this electronic transition.

These proof-of-concept simulations indicate that we have indeed achieved a generalization of the CQED approach that incorporates the molecular component in a fully *ab initio* way. At this point, we explore the numerical behavior of a true many-body formulation of the method in order to justify the use of the mean-field approximation implied by the factorization of the plasmon-molecule wave function in Eq. (11). Specifically, we compare the results of the present mean-field scheme to one in which we propagate the EOM for the two-body plasmon-electron RDM, $\rho_{B,j}^{A,i}(\xi) = \langle\Psi|\hat{b}(\xi)_A^\dagger \hat{b}(\xi)_B \hat{a}_i^\dagger \hat{a}_j|\Psi\rangle$. This EOM can be obtained from the expectation value of the commutator of the two-body operator, $\hat{b}(\xi)_A^\dagger \hat{b}(\xi)_B \hat{a}_i^\dagger \hat{a}_j$, with the Hamiltonian. In this case, the total wave function is not assumed to be a product of plasmonic and electronic wave functions, and the nanoparticle-molecule interactions are described by the two-body operator given by Eq. (5). Further details and explicit programmable expressions can be found in the Appendix.

Figure 2 illustrates the time-dependent dipole moment for Li_2 at various distances from the surface of a 20 nm gold nanoparticle. Results are presented for the mean-field and many-body formulations of CQED. Here, simulations

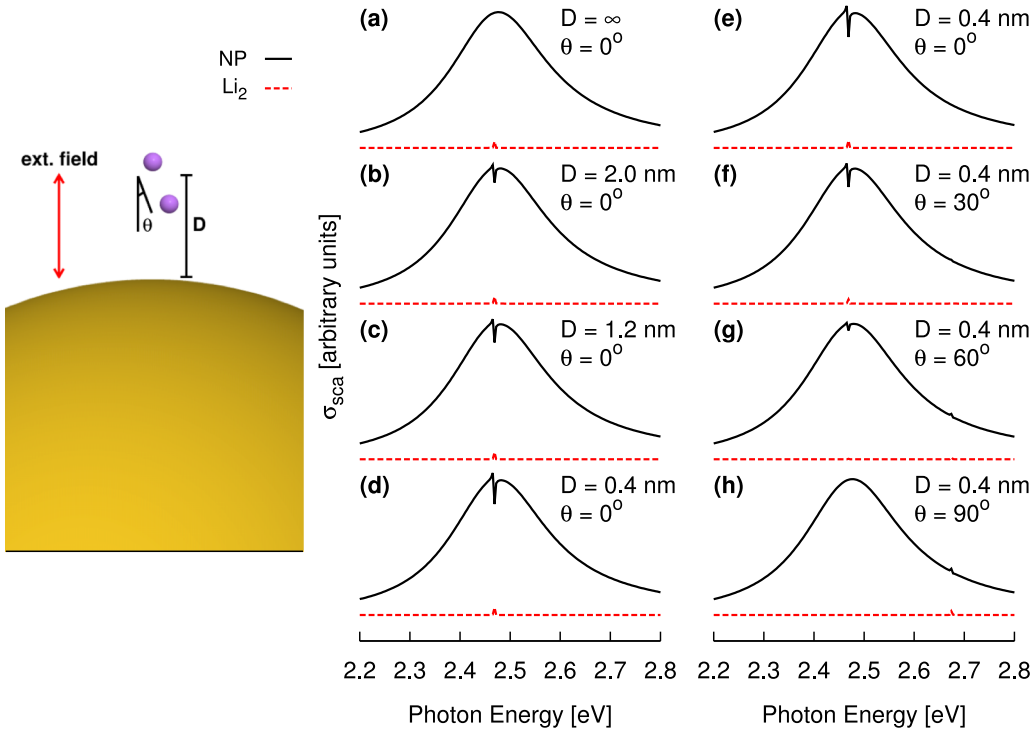

FIG. 1. Scattering cross sections for a simple molecule (Li_2, red dashed lines) coupled to a spherical gold nanoparticle (solid lines). The nanoparticle scattering cross section is strongly dependent on the molecule-nanoparticle distance (a)-(d) and the orientation of the molecule with respect to the polarization of the external electric field (e)-(h).

using both formulations include only two photon number states; the steep computational cost of the many-body variant makes simulations with large numbers of photon number states impractical. At a molecule-nanoparticle distance of 40 nm [Fig. 2(a)], the two formalisms provide a numerically indistinguishable description of the system dynamics; this is not surprising, as pure two-body plasmon-electron correlations should be negligible in the limit of infinite separation. As the molecule is brought closer to the surface of the particle, though, slight differences in the predicted time evolution of the dipole moments emerge; the phase of the dipole oscillations is slightly advanced in the case of the many-body approach. It may seem that this discrepancy could be attributed to the role of true two-body correlations, but it is much more likely that it arises from a loss of N-representability in the two-body and one-electron RDMs as evolved within the many-body formalism. An N-representable RDM is derivable from a realistic N-body wave function; the lack of N-representability here manifests itself in the increasingly negative eigenvalues of the two-body and one-electron RDMs, the lowest of which are also presented in Fig. 2. In order to fully understand this loss in N-representability, we must discuss some of the details of the many-body approach.

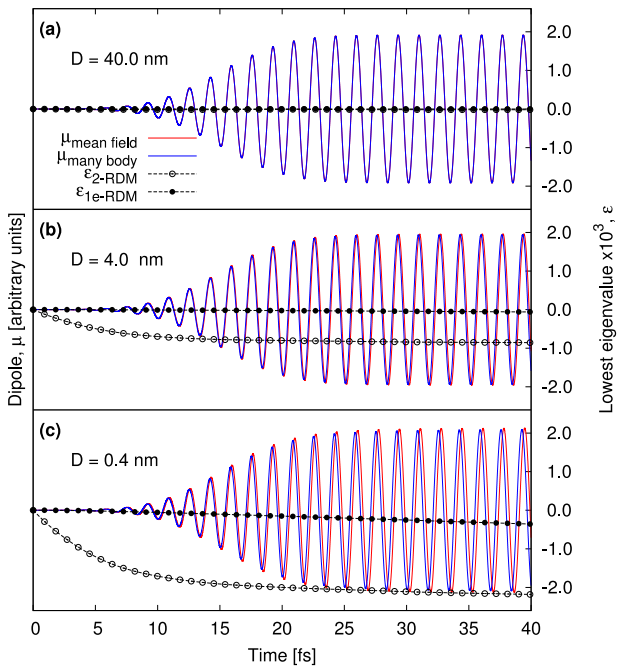

FIG. 2. Time-dependent dipole moment for Li_2 at distances of (a) 40.0 nm, (b) 4.0 nm, and (c) 0.4 nm from a 20 nm gold nanoparticle. Results are provided for the mean-field and many-body formulations of the generalized CQED method. Also shown are the lowest eigenvalues of the two-body RDM and the one-electron RDM associated with the many-body formulation of the method.

The EOM for the two-body plasmon-electron RDM depends on a three-body (plasmon-electron-electron) RDM; this dependence can be eliminated by expressing this RDM in terms of the one- and two-body RDMs[54–57] and by ignoring pure three-body correlations (see the Appendix for details). When propagating the EOM for the two-body RDM under this assumption, one cannot guarantee the preservation of the N-representability of the one- or two-body RDMs. Similar behavior has been reported previously in the context of correlated electron dynamics; for a many-electron system interacting with an oscillating electric field, the two-electron RDM rapidly becomes infeasible when its time evolution is determined by an approximate, reconstructed three-electron

RDM.[58,59] Hence, it is difficult to draw a meaningful conclusion regarding the role of two-body correlations from the data in Figs. 2(b) and 2(c); all that can be stated with certainty is that the time evolution of the two-body RDM is complicated by the reconstruction of the three-body RDM. However, the dynamical behavior of the one-body electron and plasmon RDMs according to Eqs. (21) and (24) suffers from no such problems. The mean-field approximation is then justified in the sense that it provides the only viable numerical procedure that maintains the feasibility of the reduced-density-matrices. For the remainder of this work, we consider only this mean-field CQED approach.

We now consider a coupled system composed of a larger molecule (boron-dipyrromethene, BODIPY) and a spherical silver nanoparticle with a radius of 10 nm. The plasmon resonance energy, transition dipole moment, and damping rate were initially parametrized as described in Sec. III; the plasmon excitation frequency was subsequently red-shifted to 3.35 eV, so as to have better overlap with the longitudinal $B_2 \leftarrow A_1$ excitation in BODIPY, as computed at the TDHF/6-31G level of theory. As in the simpler model system, Fig. 3 reveals the emergence of a Fano-like resonance in the limit of small molecule-nanoparticle separations. We note that, at the smallest molecule-nanoparticle distance considered (D = 0.8 nm), the actual separation between the end of the molecule and the hypothetical surface is only ≈0.3 nm; in this limit, surface effects not included in the present model may affect the time evolution of the system. However, at larger distances, these effects become less important, and the present model should capture the bulk of the interactions between the nanoparticle dipole and the molecule. As above, the transparency dip in the nanoparticle scattering cross section vanishes in the limit that the molecule and nanoparticle are infinitely separated.

Additional information regarding the interplay of the molecule and plasmon excitations can be extracted from the time-dependent dipole moments for the respective system components. Figures 4(a) and 4(c) illustrate the time evolution of the z-component of the dipole moment for the isolated nanoparticle and molecule, respectively. The plasmon decays

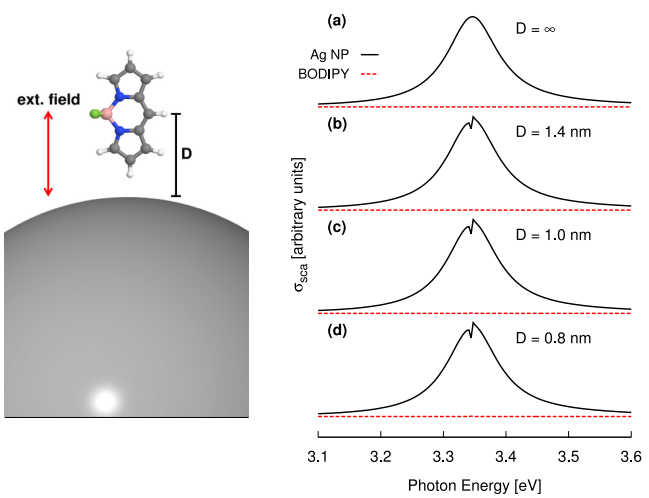

FIG. 3. Scattering cross sections for a coupled BODIPY-nanoparticle system with various molecule-nanoparticle separations.

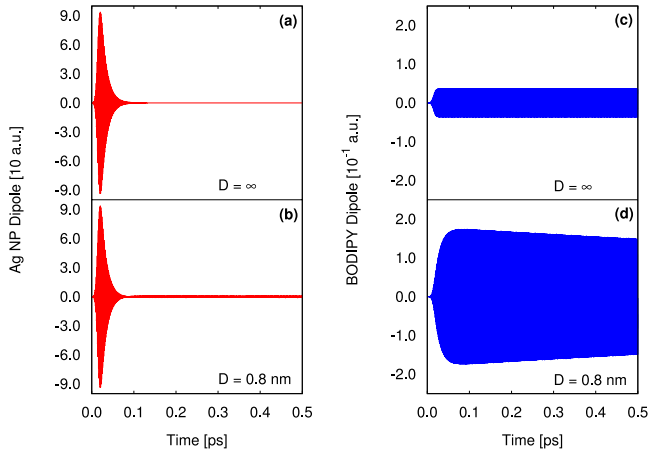

FIG. 4. Time-dependent dipole moments for (a) an isolated nanoparticle, (b) a nanoparticle resonantly coupled to BODIPY, (c) isolated BODIPY, and (d) BODIPY resonantly coupled to a nanoparticle.

within a few tens of femtoseconds after its initial excitation, whereas, because we do not include any dissipative terms in Eq. (21), the molecular excitation is infinitely long-lived. In the coupled system, the plasmon excitation again decays rapidly, but dipole oscillations persist at long times [Fig. 4(b)]. In the presence of the nanoparticle, the magnitude of the molecule dipole oscillations increases by nearly a factor of four [Fig. 4(d)], and the corresponding molecular scattering cross section is roughly 14.5 times larger than that for the isolated molecule. This increase agrees well with the local field enhancement experienced by the molecule at a distance of 0.8 nm from surface of the nanoparticle (10.8 nm from the oscillating nanoparticle dipole). The slow decay of the dipole oscillations illustrated in Fig. 4(d) indicates an indirect damping of the molecular excitation through molecule-nanoparticle coupling; recall, the present approach includes no direct channel for molecular dissipation.

The strongly damped oscillations in the dipole manifold for the nanoparticle presented in Fig. 4(b) indicate an incomplete vacuum Rabi cycle. This phenomenon can arise when a quantum emitter and a cavity alternatively exchange photons; in the case of a two-level emitter, the system oscillates between states $|A_\xi\rangle|g\rangle$ and $|A_\xi - 1\rangle|e\rangle$, where $|g\rangle$ and $|e\rangle$ represent the ground and excited states of the emitter, respectively. Prior to the minimum in the dipole manifold for the nanoparticle (≈85 fs), oscillations in the nanoparticle dipole moment drive an electronic excitation in BODIPY; after this point, the excited molecule has the potential to drive an excitation in the nanoparticle. However, in the present case, the rate of energy dissipation is greater than the rate of energy transfer from the molecule to the nanoparticle, and the system sustains only the first half of the Rabi cycle.

This behavior is reflected in the relative phases of the induced dipoles of the molecule and nanoparticle. At early times, the plasmon excitation is driven by the external electric field, and the nanoparticle dipole lags behind the external field with a $\pi/2$ phase difference. The plasmon rapidly becomes the main driver of the molecular excitation, which leads to a similar $\pi/2$ phase lag between the molecule and nanoparticle dipole moments ($\Delta\phi$ in Fig. 5). This phase relationship is well

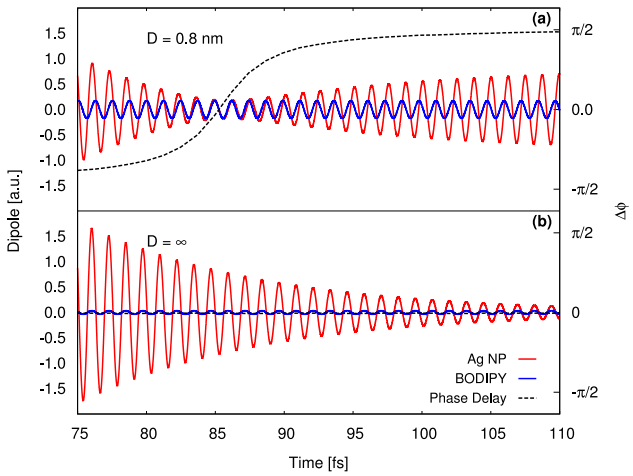

FIG. 5. Time-dependent dipole moments for the molecular and plasmonic components of (a) coupled and (b) infinitely separated systems. The dashed line indicates the relative phase of the dipole moments, $\Delta\phi$; for the coupled system, a phase shift at roughly 85 fs signals the completion of the first half of a vacuum Rabi cycle.

established by the end of the laser pulse. At the minimum in the dipole manifold, a shift in the relative phases of the molecule and nanoparticle induced dipole moments occurs, and the molecule and nanoparticle maintain this phase relationship for the remainder of the simulation. This behavior contrasts with that of the isolated molecule and nanoparticle [Fig. 5(b)]. Here, the system components are uncoupled, and both induced dipoles oscillate in phase at all times (and always $\pi/2$ out of phase with the external electric field).

The phase information presented in Fig. 6 indicates that the time-to-phase reversal decreases with decreasing nanoparticle-molecule distances. In another way, the molecule-nanoparticle coupling strength increases with decreasing nanoparticle-molecule distance; the increase in the coupling strength manifests itself in a higher Rabi frequency and a shorter time-to-phase reversal. In the distance range explored, the time-to-phase reversal depends nearly linearly on the molecule-nanoparticle distance, suggesting that this feature could, in principle, serve as a sort of molecular ruler.

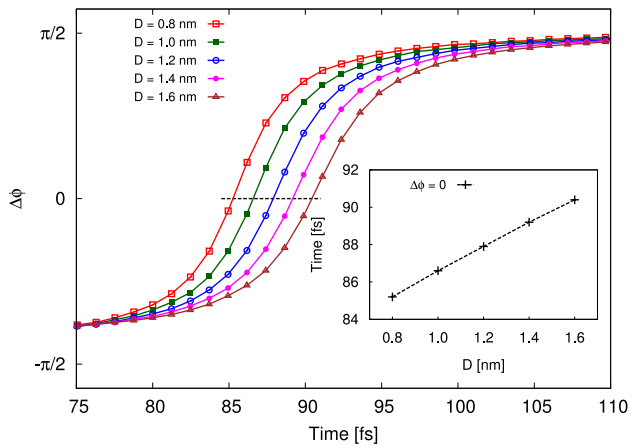

FIG. 6. The relative phase of the time-dependent molecule and nanoparticle dipole moments for several molecule-nanoparticle separations. The inset indicates that the time-to-phase reversal varies linearly with this separation.

V. CONCLUSIONS

We have introduced an *ab initio* electronic Hamiltonian into the CQED formalism to simulate molecule-plasmon interactions. This approach goes beyond the usual two-level treatment of quantum emitters in CQED. Practically solvable equations of motion were derived by considering only mean-field interactions between electrons and between the electronic and plasmonic components; the inclusion of true two-body plasmon-electron correlations leads to a numerical procedure that cannot maintain the feasibility of the reduced-density-matrices. The resulting fully quantum-mechanical approach offers a simple and computationally efficient method to simulate both ground-state and time-dependent molecule-nanoparticle interactions. Mutual polarization effects are easily incorporated into ground-state self-consistent field computations at very little cost, and the computational scaling of the time evolution of the coupled system is comparable to that of a conventional real-time TDHF simulation; the formalism will be straightforward to extend to real-time time-dependent density-functional theory. The description of the plasmonic system components can easily be generalized to include either multiple plasmonic particles or higher-order multipole contributions to the interaction Hamiltonian. Further, because the plasmon excitation is treated in a quantum-mechanical way, this approach can be used to study entanglement between plasmon and molecular excitations or between excitations in multiple plasmonic particles.[45]

The formalism presented herein was used to explore the emergence of Fano-like resonances in general molecule-nanoparticle complexes where the plasmon resonance energy overlapped with bright molecular excitations. The resulting line shapes were found to be quite sensitive to the molecule-nanoparticle distance and the relative orientation of the molecule and the polarization of the external electric field. Strongly damped oscillations in the dipole manifold for the nanoparticle and a reversal of the relative phases of the nanoparticle and molecule dipole moments indicate a vacuum Rabi cycle; only the first half of the cycle is observed, because of the rapid dissipation of the plasmon excitation. The coupling strength and Rabi frequency increase with decreasing molecule-nanoparticle distances; for BODIPY-nanoparticle distances in the range of 0.8–1.6 nm, the time-to-phase reversal depends linearly on this separation. In principle, measurable changes in this feature could be leveraged in the context of molecule-scale rulers.

ACKNOWLEDGMENTS

The authors acknowledge financial support from the Department of Chemistry and Biochemistry at Florida State University and the American Chemical Society Petroleum Research Fund (Grant No. 54668-DNI6).

APPENDIX: TWO-BODY PLASMON-ELECTRON CORRELATIONS

The plasmon-electron two-body RDM (2-RDM), $\rho^{A,i}_{B,j}(\xi) = \langle\Psi|\hat{b}(\xi)^\dagger_A \hat{b}(\xi)_B \hat{a}^\dagger_i \hat{a}_j|\Psi\rangle$, describes correlations between

electrons and plasmons, and the diagonal elements of this tensor are related to the simultaneous probability of finding an electron in a given orbital and a plasmon mode in a particular photon number state. The EOM for this 2-RDM is given by the commutator of the two-body density operator with the total time-dependent Hamiltonian, $\hat{H}(t)$,

$$i\frac{d}{dt}\rho^{A,i}_{B,j}(\xi) = \langle\Psi|[\hat{b}(\xi)^\dagger_A\hat{b}(\xi)_B\hat{a}^\dagger_i\hat{a}_j, \hat{H}(t)]|\Psi\rangle, \tag{A1}$$

where

$$\hat{H}(t) = \hat{H}_0 - \left(\hat{\boldsymbol{\mu}}_\mathrm{e} + \hat{\boldsymbol{\mu}}_\mathrm{p}\right)\cdot\mathcal{E}(t). \tag{A2}$$

If the molecule-nanoparticle interaction term included in $\hat{H}_0$ is the two-body operator given by Eq. (5), then this EOM will capture true two-body plasmon-electron correlations. The right-hand side of Eq. (A1) is a function of one-, two-, and three-body RDMs,

$$\begin{aligned}
i\frac{d}{dt}\rho^{A,i}_{B,j}(\xi) = &\sum_p\left[\rho^{A,i}_{B,p}(\xi)\left(h_{jp} - \mu^\xi_{jp}\mathcal{E}(\xi,t)\right) - \rho^{A,p}_{B,j}(\xi)\left(h_{pi} - \mu^\xi_{pi}\mathcal{E}(\xi,t)\right)\right]\\
&+ \sum_{p,q,r}\left(\rho^{A,i,q}_{B,p,r}(\xi)(jp|qr) - \rho^{A,q,p}_{B,r,j}(\xi)(pi|qr)\right) + \rho^{A,i}_{B,j}(\xi)\,(A-B)\,\omega^\xi_\mathrm{p}\\
&- \left(\rho^{A,i}_{B-1,j}(\xi)\sqrt{B} + \rho^{A,i}_{B+1,j}(\xi)\sqrt{B+1} - \rho^{A-1,i}_{B,j}(\xi)\sqrt{A} - \rho^{A+1,i}_{B,j}(\xi)\sqrt{A+1}\right)\mu^\xi_\mathrm{p}\mathcal{E}(\xi,t)\\
&- \frac{2\mu^\xi_\mathrm{p}}{|\xi_\mathrm{e}-\xi_\mathrm{p}|^3}\left\{\sum_p\left[\left(\rho^{A,i}_{B-1,p}(\xi)\sqrt{B} + \rho^{A,i}_{B+1,p}(\xi)\sqrt{B+1}\right)\mu^\xi_{pj} - \left(\rho^{A-1,p}_{B,j}(\xi)\sqrt{A} - \rho^{A+1,p}_{B,j}(\xi)\sqrt{A+1}\right)\mu^\xi_{ip}\right]\right.\\
&\left.+ \sum_{p,q}\left(\rho^{A,i,p}_{B-1,j,q}(\xi)\sqrt{B} + \rho^{A,i,p}_{B+1,j,q}(\xi)\sqrt{B+1} - \rho^{A-1,i,p}_{B,j,q}(\xi)\sqrt{A} - \rho^{A+1,i,p}_{B,j,q}(\xi)\sqrt{A+1}\right)\mu^\xi_{pq}\right\},
\end{aligned} \tag{A3}$$

and the time-derivative of the two-body RDM is hence indeterminate without knowledge of the three-body RDM, or some approximation to it, at each time step.

Cumulant decompositions of high-order RDMs are often employed in the context of ground-state electronic structure computations to remove similar indeterminacies.[54–57] The two-body RDM can be expressed as

$$\rho^{A,p}_{B,q}(\xi) = \rho^A_B(\xi)\,\rho^p_q + {}^2\Delta^{A,p}_{B,q}(\xi), \tag{A4}$$

where the symbol ${}^2\Delta^{A,p}_{B,q}(\xi)$ denotes the two-body plasmon-electron cumulant matrix, which represents pure two-body correlations and cannot be expressed in terms of products of lower RDMs. The three-body RDM can be expressed as

$$\rho^{A,p,r}_{B,q,s}(\xi) = \rho^A_B(\xi)\,\rho^p_q\wedge\rho^r_s + 3\,{}^2\Delta^{A,p}_{B,q}(\xi)\wedge\rho^r_s + {}^3\Delta^{A,p,r}_{B,q,s}(\xi), \tag{A5}$$

where the symbol, $\wedge$, denotes an antisymmetric tensor product, for example, $\rho^p_q\wedge\rho^r_s = \rho^p_q\rho^r_s - \rho^p_s\rho^r_q$. Note that fermion-boson exchanges are not included, as $\rho^A_q = 0$.

In order to obtain a set of programmable equations, we make the following two assumptions:

1. The electron-electron correlations are assumed to be negligible, implying
$$ {}^2\Delta^{p,r}_{q,s} = 0; \tag{A6}$$
in practice, this assumption leads to a mean-field description of electron-electron interactions.
2. Since two-body correlations are assumed to be negligible, it is reasonable to also neglect pure three-body correlations, implying
$$ {}^3\Delta^{A,p,r}_{B,q,s}(\xi) = 0. \tag{A7}$$

The general form of the 3-RDM then becomes

$$\begin{aligned}
\rho^{A,p,r}_{B,q,s}(\xi) = &\rho^{A,p}_{B,q}(\xi)\rho^r_s + \rho^{A,r}_{B,s}(\xi)\rho^p_q - \rho^A_B(\xi)\rho^r_s\rho^p_q\\
&- \rho^{A,p}_{B,s}(\xi)\rho^r_q - \rho^{A,r}_{B,q}(\xi)\rho^p_s + \rho^A_B(\xi)\rho^r_q\rho^p_s,
\end{aligned} \tag{A8}$$

and a programmable EOM for the 2-RDM, which still includes two-body electron-plasmon correlations, can be obtained by plugging Eq. (A8) into Eq. (A3). The evaluation of the time derivative of the 2-RDM can be performed with $\mathcal{O}(N_\mathrm{p}^2N_\mathrm{e}^4)$ floating point operations, where N_p and N_e represent the number of plasmon photon number states and the number of one-electron basis functions, respectively. For computations involving only a small number of photon number states (say, 2-3), the computational cost of this procedure is roughly an order of magnitude more expensive than a conventional real-time TDHF simulation of the isolated molecular component. For larger numbers of photon number states, which are necessary when considering strong external electric fields, computations become prohibitively expensive.

Further simplifications drastically reduce the computational cost of this approach. For example, by splitting the interaction term into the two contributions given in Eqs. (13) and (14) and assuming that the total wave function is separable into a product of plasmonic and electronic wave functions, the computational scaling of the approach can be reduced to $\mathcal{O}(N_\mathrm{p}^2) + \mathcal{O}(N_\mathrm{e}^4)$. By restricting our model for the system to a product wave function, we imply that ${}^2\Delta^{A,p}_{B,q}(\xi) = 0$, and much simpler equations of motion can be obtained by considering the time evolution of the 1-body plasmon and electron RDMs separately. Upon evaluation of the commutators in Eqs. (21) and (22), we obtain the following expressions:

$$i\frac{d}{dt}\rho_B^A(\xi) = \rho_B^A(\xi)\,(A-B)\,\omega_{\rm p}^{\xi} - \left(\rho_{B-1}^A(\xi)\sqrt{B} + \rho_{B+1}^A(\xi)\sqrt{B+1} - \rho_B^{A-1}(\xi)\sqrt{A} - \rho_B^{A+1}(\xi)\sqrt{A+1}\right)\left(\mu_{\rm p}^{\xi}\mathcal{E}(\xi,t) + \frac{2\mu_{\rm p}^{\xi}\langle\mu_{pq}^{\xi}\rangle}{|\xi_{\rm e}-\xi_{\rm p}|^3}\right), \tag{A9}$$

and

$$i\frac{d}{dt}\rho_j^i = \sum_p \left[\rho_p^i\left(h_{jp} + J_j^p - K_j^p + V_j^p - \sum_{\xi}\mu_{jp}^{\xi}\mathcal{E}(\xi,t)\right) - \rho_j^p\left(h_{pi} + J_p^i - K_p^i + V_p^i - \sum_{\xi}\mu_{pi}^{\xi}\mathcal{E}(\xi,t)\right)\right], \tag{A10}$$

where J_q^p and K_q^p are the usual Coulomb and exchange matrices, and V_q^p is the matrix representation of the operator $\hat{H}_{\rm i}^{\rm p\to e}$, expressed in the one-electron basis set. Equation (A10) is essentially the EOM according to time-dependent Hartree-Fock theory, augmented by the potential due to the presence of the nanoparticle dipole moment.

As described in Sec. II B, the decay of the plasmon excitation is incorporated via the Lindblad formalism, and the relevant expressions are

$$\begin{aligned}\langle\Psi|\hat{L}(\hat{b}(\xi)_A^{\dagger}\hat{b}(\xi)_B\hat{a}_i^{\dagger}\hat{a}_j)|\Psi\rangle &= -\frac{\gamma_{\rm p}^{\xi}}{2}\,(A+B)\,\rho_{B,j}^{A,i}(\xi) \\ &\quad + \gamma_{\rm p}^{\xi}\left[(A+1)(B+1)\right]^{1/2}\rho_{B+1,j}^{A+1,i}(\xi),\end{aligned} \tag{A11}$$

and

$$\begin{aligned}\langle\Psi|\hat{L}(\hat{b}(\xi)_A^{\dagger}\hat{b}(\xi)_B)|\Psi\rangle &= -\frac{\gamma_{\rm p}^{\xi}}{2}\,(A+B)\,\rho_B^A(\xi) \\ &\quad + \gamma_{\rm p}^{\xi}\left[(A+1)(B+1)\right]^{1/2}\rho_{B+1}^{A+1}(\xi),\end{aligned} \tag{A12}$$

in the many-body and mean-field approaches, respectively.

[1]D. L. Jeanmaire and R. P. Van Duyne, J. Electroanal. Chem. Interfacial Electrochem. **84**, 1 (1977).
[2]M. G. Albrecht and J. A. Creighton, J. Am. Chem. Soc. **99**, 5215 (1977).
[3]S. Nie and S. R. Emory, Science **275**, 1102 (1997).
[4]C. L. Haynes, C. R. Yonzon, X. Zhang, and R. P. Van Duyne, J. Raman Spectrosc. **36**, 471 (2005).
[5]C. E. Talley, J. B. Jackson, C. Oubre, N. K. Grady, C. W. Hollars, S. M. Lane, T. R. Huser, P. Nordlander, and N. J. Halas, Nano Lett. **5**, 1569 (2005).
[6]F. Le, D. W. Brandl, Y. A. Urzhumov, H. Wang, J. Kundu, N. J. Halas, J. Aizpurua, and P. Nordlander, ACS Nano **2**, 707 (2008).
[7]R. Antoine, P. F. Brevet, H. H. Girault, D. Bethell, and D. J. Schiffrin, Chem. Commun. **1997**, 1901–1902.
[8]P. Genevet, J.-P. Tetienne, E. Gatzogiannis, R. Blanchard, M. A. Kats, M. O. Scully, and F. Capasso, Nano Lett. **10**, 4880 (2010).
[9]W. L. Barnes, J. Mod. Opt. **45**, 661 (1998).
[10]J. R. Lakowicz, Anal. Biochem. **298**, 1 (2001).
[11]E. Balan, F. Mauri, C. Lemaire, C. Brouder, F. Guyot, A. M. Saitta, and B. Devouard, Phys. Rev. Lett. **89**, 177401 (2002).
[12]J. Lee, A. O. Govorov, J. Dulka, and N. A. Kotov, Nano Lett. **4**, 2323 (2004).
[13]K. Ray, R. Badugu, and J. R. Lakowicz, J. Am. Chem. Soc. **128**, 8998 (2006).
[14]J. R. Lakowicz, Plasmonics **1**, 5 (2006).
[15]F. Tam, G. P. Goodrich, B. R. Johnson, and N. J. Halas, Nano Lett. **7**, 496 (2007).
[16]R. Bardhan, N. K. Grady, J. R. Cole, A. Joshi, and N. J. Halas, ACS Nano **3**, 744 (2009).
[17]R. A. Shah, N. F. Scherer, M. Pelton, and S. K. Gray, Phys. Rev. B **88**, 075411 (2013).
[18]W. Zhang, A. O. Govorov, and G. W. Bryant, Phys. Rev. Lett. **97**, 146804 (2006).
[19]A. Ridolfo, O. Di Stefano, N. Fina, R. Saija, and S. Savasta, Phys. Rev. Lett. **105**, 263601 (2010).
[20]E. Waks and D. Sridharan, Phys. Rev. A **82**, 043845 (2010).
[21]X. Wu, S. K. Gray, and M. Pelton, Opt. Express **18**, 23633 (2010).
[22]B. N. J. Persson and N. D. Lang, Phys. Rev. B **26**, 5409 (1982).
[23]T. L. Jennings, M. P. Singh, and G. F. Strouse, J. Am. Chem. Soc. **128**, 5462 (2006).
[24]A. O. Govorov, G. W. Bryant, W. Zhang, T. Skeini, J. Lee, N. A. Kotov, J. M. Slocik, and R. R. Naik, Nano Lett. **6**, 984 (2006).
[25]B. T. Draine and P. J. Flatau, J. Opt. Soc. Am. A **11**, 1491 (1994).
[26]A. Taflove and S. C. Hagness, *Computational Electrodynamics: The Finite-Difference Time-Domain Method*, 3rd ed. (Artech House, 2005), ISBN: 978-1580538329.
[27]H. Chen, J. M. McMahon, M. A. Ratner, and G. C. Schatz, J. Phys. Chem. C **114**, 14384 (2010).
[28]J. Mullin, N. Valley, M. G. Blaber, and G. C. Schatz, J. Phys. Chem. A **116**, 9574 (2012).
[29]D. Neuhauser and K. Lopata, J. Chem. Phys. **127**, 154715 (2007).
[30]K. Lopata and D. Neuhauser, J. Chem. Phys. **131**, 014701 (2009).
[31]G. C. des Francs, C. Girard, T. Laroche, G. Lévèque, and O. J. F. Martin, J. Chem. Phys. **127**, 034701 (2007).
[32]D. J. Masiello and G. C. Schatz, Phys. Rev. A **78**, 042505 (2008).
[33]D. J. Masiello and G. C. Schatz, J. Chem. Phys. **132**, 064102 (2010).
[34]J. P. Litz, R. P. Brewster, A. B. Lee, and D. J. Masiello, J. Phys. Chem. C **117**, 12249 (2013).
[35]D. J. Masiello, Int. J. Quantum Chem. **114**, 1413 (2014).
[36]S. Corni and J. Tomasi, J. Chem. Phys. **114**, 3739 (2001).
[37]S. Corni and J. Tomasi, J. Chem. Phys. **116**, 1156 (2002).
[38]O. Andreussi, S. Corni, B. Mennucci, and J. Tomasi, J. Chem. Phys. **121**, 10190 (2004).
[39]S. Corni and J. Tomasi, J. Chem. Phys. **117**, 7266 (2002).
[40]S. Vukovic, S. Corni, and B. Mennucci, J. Phys. Chem. C **113**, 121 (2009).
[41]A. Muñoz Losa, S. Vukovic, S. Corni, and B. Mennucci, J. Phys. Chem. C **113**, 16364 (2009).
[42]J. Fosso-Tande and R. J. Harrison, Comput. Theor. Chem. **1017**, 22 (2013).
[43]R. D. Artuso and G. W. Bryant, Nano Lett. **8**, 2106 (2008).
[44]E. B. Flagg, A. Muller, J. W. Robertson, S. Founta, D. G. Deppe, M. Xiao, W. Ma, G. J. Salamo, and C. K. Shih, Nat. Phys. **5**, 203 (2009).
[45]N. Thakkar, C. Cherqui, and D. J. Masiello, ACS Photonics **2**, 157 (2015).
[46]E. Jaynes and F. W. Cummings, Proc. IEEE **51**, 89 (1963).
[47]G. Lindblad, Commun. Math. Phys. **48**, 119 (1976).
[48]J. M. Turney, A. C. Simmonett, R. M. Parrish, E. G. Hohenstein, F. A. Evangelista, J. T. Fermann, B. J. Mintz, L. A. Burns, J. J. Wilke, M. L. Abrams *et al.*, Wiley Interdiscip. Rev.: Comput. Mol. Sci. **2**, 556 (2012).
[49]P. B. Johnson and R. W. Christy, Phys. Rev. B **6**, 4370 (1972).
[50]L. Novotny and B. Hecht, *Principles of Nano-Optics* (Cambridge University Press, 2006), ISBN: 9780511813535.
[51]M. König, M. Rahmani, L. Zhang, D. Y. Lei, T. R. Roschuk, V. Giannini, C.-W. Qiu, M. Hong, S. Schlücker, and S. A. Maier, ACS Nano **8**, 9188 (2014).
[52]Y. Zhang, Y.-R. Zhen, O. Neumann, J. K. Day, P. Nordlander, and N. J. Halas, Nat. Commun. **5**, 4424 (2014).
[53]K. C. Woo, L. Shao, H. Chen, Y. Liang, J. Wang, and H.-Q. Lin, ACS Nano **5**, 5976 (2011).
[54]F. Colmenero and C. Valdemoro, Phys. Rev. A **47**, 979 (1993).
[55]H. Nakatsuji and K. Yasuda, Phys. Rev. Lett. **76**, 1039 (1996).
[56]D. A. Mazziotti, Chem. Phys. Lett. **289**, 419 (1998).
[57]W. Kutzelnigg and D. Mukherjee, J. Chem. Phys. **110**, 2800 (1999).
[58]B. Schäfer-Bung and M. Nest, Phys. Rev. A **78**, 012512 (2008).
[59]A. Akbari, M. J. Hashemi, A. Rubio, R. M. Nieminen, and R. van Leeuwen, Phys. Rev. B **85**, 235121 (2012).